

Variable-Temperature Scattering and Spectroscopy Characterizations for Temperature-Dependent Solution Assembly of PffBT4T-Based Conjugated Polymers

Zhiqiang Cao, Guorong Ma, Mingwan Leng, Song Zhang, Jihua Chen, Changwoo Do, Kunlun Hong, Lei Fang, and Xiaodan Gu*



Cite This: *ACS Appl. Polym. Mater.* 2022, 4, 3023–3033



Read Online

ACCESS |

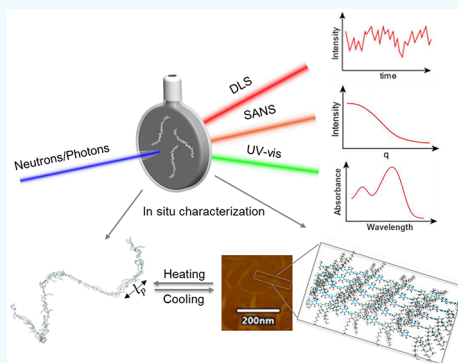
Metrics & More

Article Recommendations

Supporting Information

ABSTRACT: The solution structure of conjugated polymers (CPs) from which the films are cast is critical for tailoring the thin-film morphology thus device performance. Here, we used multimodal variable-temperature scattering and spectroscopy tools to fully quantify the solution assembly of poly[(5,6-difluoro-2,1,3-benzothiadiazol-4,7-diyl)-*alt*-(3,3"-dialkyl-2,2';5',2";5",2""-quaterthiophen-5,5""-diyl)] (PffBT4T) polymers with varying side-chain lengths at different assembly temperatures. The conformational and aggregation behaviors for PffBT4T-based CPs were found to be very sensitive to both temperature and side chain length using ultraviolet–visible (UV–vis) spectroscopy, nuclear magnetic resonance (NMR) spectroscopy, dynamic light scattering (DLS), and small-angle neutron scattering (SANS). We found that with slightly increasing side chain length from 2-octyldodecyl (C8C12) to 2-nonyltridecyl (C9C13), PffBT4T-based CPs show a significant decrease in aggregation-to-dissolved chain transition temperature (10 °C), degree of aggregation, enthalpy change of aggregation, and size of the aggregates in solution. At room temperature, PffBT4T polymer strongly aggregated to form fabric structure with the film thickness of a few nanometers in thickness and hundreds of nanometers in length, as probed by atomic force microscopy (AFM), transmission electronic microscopy (TEM), and dynamic light scattering (DLS). At the elevated temperature above the aggregation-to-dissolved chain transition temperature, PffBT4T is fully dissolved and adopts a semiflexible coil conformation with the persistence length of 3.1 nm for PffBT4T-C8C12 and a slightly increased persistence length of 3.4 nm for PffBT4T-C9C13, according to temperature-dependent SANS measurements. Longer side chains of PffBT4T-C9C13 also lead to less aggregation enthalpy gain compared with PffBT4T-C8C12. This work provides a solution structure manipulating strategy of CPs and thus will inspire the molecular design and processing protocols of CPs toward higher performance electronic devices.

KEYWORDS: conjugated polymers, small-angle neutron scattering, chain conformation, polymer aggregation, side-chain length



INTRODUCTION

The ease of solution processing of conjugated polymers (CPs) makes them widely adopted in optoelectronic devices, such as photovoltaics (OPVs),^{1,2} organic light-emitting diode (OLED),³ transistors,^{4–6} and other emerging applications.^{7,8} Significant advances have been achieved such as power conversion efficiency (PCE) for OPVs exceeding 18%,^{2,9,10} charge carrier mobilities catching up with inorganic counterparts, e.g., amorphous silicon.¹¹ Despite the significant advances in device engineering and optimization, the fundamental principles underlying the solution property of functional conjugated polymeric ink and the fabrication of high-performance devices based on these inks are far from fully understood.

Understanding the morphology of CPs in solution and its rapid evolution during solution processing is the cornerstone for optimizing the optoelectronic performance, and it provides

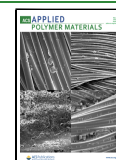
reliable and reproducible control of the final device morphology.^{12,13} Most solution processing processes, such as spin coating and blade coating, involve rapid solvent evaporation during the film drying process. Thus, polymers are commonly trapped in morphology that is far from equilibrium. Consequently, the assembled structure for CPs in solution strongly influences the solid-phase morphology and device performance. However, the lack of understanding concerning the hierarchical assembly of CPs in the solution hinders this field from fully unleashing all the potential for

Special Issue: Early Career Forum

Received: November 1, 2021

Accepted: January 25, 2022

Published: February 9, 2022



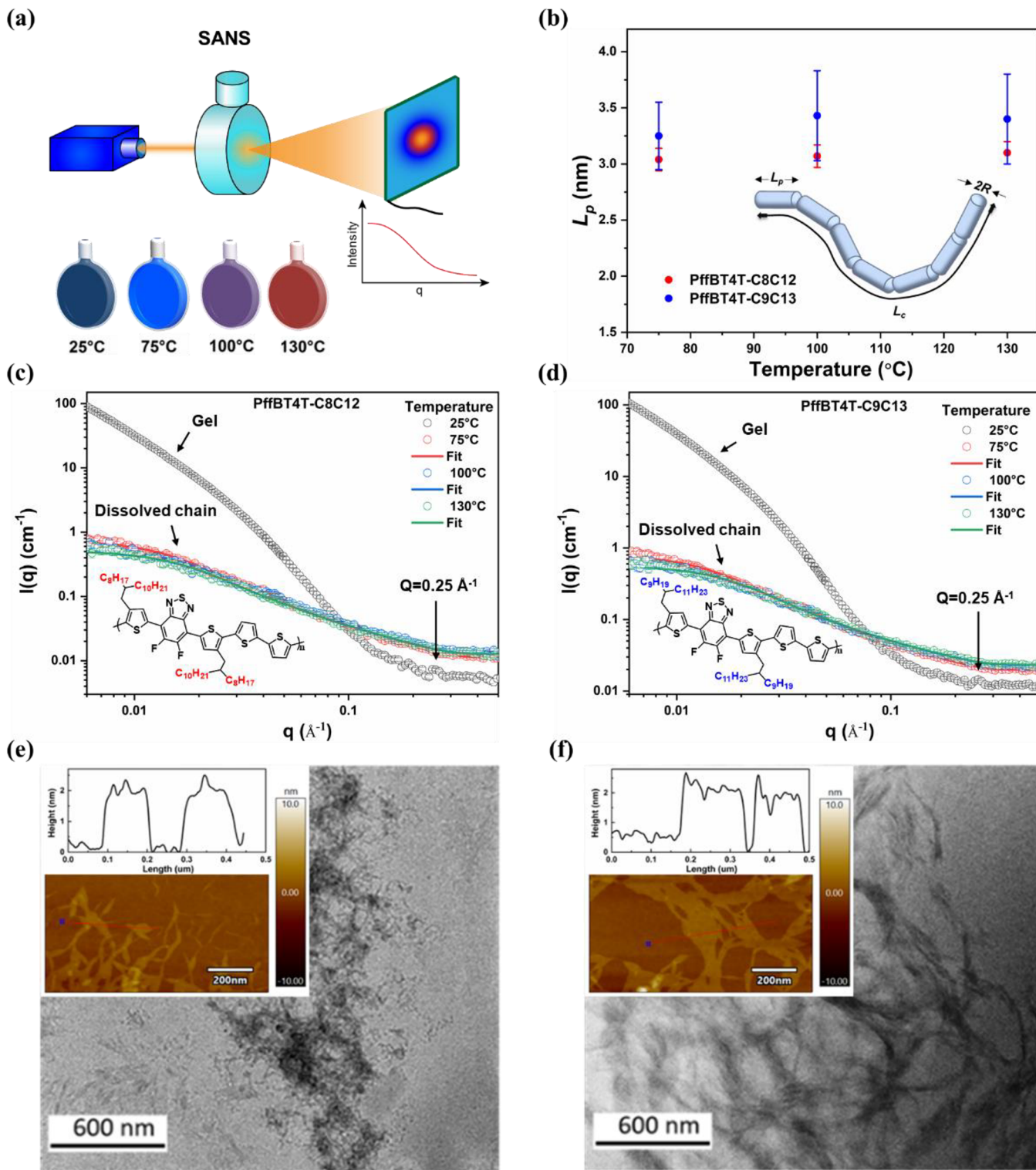


Figure 1. Solution aggregation property of PffBT4T polymer probed by solution SANS, and microscopy. (a) Schematic of variable-temperature solution SANS. (b) l_p for PffBT4T-C8C12 and PffBT4T-C9C13 at elevated temperatures. The inset figure is a schematic illustration representing a flexible cylinder model. Temperature-dependent SANS profile of PffBT4T-C8C12 (c) and PffBT4T-C9C13 (d) in *o*-DCB-*d*₄ at a concentration of 5 mg/mL. TEM image of aggregates by drop-casting the (e) PffBT4T-C8C12 solution and (f) PffBT4T-C8C12 solution (0.1 mg/mL, in *o*-DCB). Inset is AFM height images and height profile of a line cut of the aggregates, scale bar is 200 nm.

solution-processed electronic devices. In solution states, CPs strongly interact with each other, are rarely fully dissolved, and often form aggregates at room temperature.

Reported research works on single-chain conformation limited to the early developed CPs including poly(3-alkyl

thiophenes)^{14,15} (P3ATs), poly(2,3-diphenylphenylenevinylene),^{16–18} polyfluorenes.^{19–21} Until recently, chain rigidity of high-performance donor–acceptor CPs, like poly[[4,8-bis[(2-ethylhexyl)oxy]benzo[1,2-*b*:4,5-*b*']dithiophene-2,6-diyl][3-fluoro-2-[(2-ethylhexyl)carbonyl]thieno[3,4-*b*]-

thiophenediyl]] (PTB7),²² diketopyrrolopyrrole (DPP) derivatives,^{23,24} and benzodifurandione oligo(p-phenylenevinylene) (BDOPV)-based polymers,^{25,26} started to attract attention. The formation of fiber-like aggregates for P3ATs,^{24,27–30} and sheet-like aggregates for polyfluorenes,³¹ nanoribbons, or amorphous aggregates for DPP-based polymers,^{23,24} have been observed. The primary aggregates can evolve further and form loosely packed structure up to a micrometer scale,²³ and even self-assemble into large colloidal structures that span tens of micrometers.^{28,32} The aggregation of CPs also raised strong interest as the aggregates significantly impact optoelectronic properties.³³ For example, aggregated P3ATs showed a significant red shift in their absorption spectroscopy compared to the dissolved chain. Currently, no clear understanding of the relationship between molecular structure and conformation has been obtained, including the influence of the side-chain structure on CP's chain conformation.³⁴

In 2014, Yan He and co-workers reported CPs based on quaterthiophene (4T) and (difluorinated) benzothiadiazole (BT) (PffBT4T), that enabled high-efficiency polymer solar cells (>10%).³⁵ In particular, fine-tuning the length of alkyl chains of PffBT4T-based polymers can dramatically influence the efficiency of fabricated solar cell devices.¹ Notably, PffBT4T-C9C13 polymer (see molecular structure in Figure 1) was adopted to achieve a record-high power conversion efficiency by altering the alkyl chains from 2-octyldodecyl (C8C12) (average PCE of 9.2%) alkyl chains to 2-nonyltridecyl (C9C13) (average PCE of 11.3%) alkyl chains.¹ The high performance was credited to fine-tuning aggregation properties and blend morphology when processing the polymer solution (5–10 mg/mL) at moderately elevated temperatures (e.g., 60–80 °C).^{35,36} Nevertheless, at the fundamental level, it is unclear that how the alkyl-chain length impacts the conformational and aggregation structure in solution for PffBT4T-based polymers.

In this work, the conformation and aggregation behavior of PffBT4T-based polymers with two side chain lengths (from C8C12 to C9C13) in solution at different temperatures were investigated by a suite of variable-temperature scattering and spectroscopy tools including, ultraviolet–visible (UV–vis) spectroscopy, small-angle neutron scattering (SANS), dynamic light scattering (DLS), and nuclear magnetic resonance (NMR) spectroscopy. We observed that PffBT4T polymers formed large aggregates below the aggregation-to-dissolved chain transition temperature, but dissolved down to the molecular level and adopted a semiflexible coil conformation above the transition temperature at a wide range of polymer concentration from 0.05 to 5 mg/mL in ortho dichlorobenzene. The size of aggregates and degree of aggregation is highly dependent on temperature and side-chain length. At the same temperature, the size of primary aggregates and degree of aggregation decreases with increasing side-chain length, indicating the longer side chain hinders the growth of aggregates. The Van't Hoff analysis indicated that longer side chains of PffBT4T-C9C13 lead to less enthalpy gain compared with PffBT4T-C8C12. The side chain length also influences the chain conformation for fully dissolved PffBT4T at elevated temperatures, with persistence length (l_p) at 3.1 nm for PffBT4T-C8C12 versus 3.4 nm for PffBT4T-C9C13. The sheet-like primary aggregates (thickness of 2–3 nm) of PffBT4T-based polymers were confirmed by TEM and AFM for deposited films. The primary aggregates can self-assemble

into loosely packed objects and even nonflowing gel in solution at room temperature. Our multimodal variable-temperature scattering and spectroscopy experiment suggested that rich morphology can be formed for CPs in solution and side chain length offers a straightforward way to fine-tune solution assembly of CPs.

METHODS

Materials. PffBT4T-based polymers were purchased from Sigma-Aldrich. *o*-Dichlorobenzene (*o*-DCB), and deuterated *o*-dichlorobenzene (*o*-DCB-*d*₄) were also purchased from Sigma-Aldrich and used without further purification.

Gel Permeation Chromatography (GPC). The number-average molecular weight (M_n) and dispersity (D) were determined relative to polystyrene standards at 160 °C in 1,2,4-trichlorobenzene (stabilized with 125 ppm of butylated hydroxytoluene) using an Agilent PL-GPC 220 high-temperature GPC/SEC system equipped with four PLgel 10 μm MIXED-B columns.

Thermogravimetry Analysis (TGA). TGA measurements were performed on Mettler Toledo TGA with a heating rate of 10 °C/min under an inert nitrogen gas atmosphere.

Differential Scanning Calorimetry (DSC). DSC measurements were performed with a Mettler Toledo DSC 3+. The samples were first heated above their melting temperature (300 °C) followed by cooling to –90 °C with a rate of 10 °C/min. After that, the samples were heated at the same rate. The DSC data were taken at the cooling and second reheating scans for determining crystallization temperature, melting temperature, and melting enthalpy.

UV–Vis Spectroscopy. Temperature-dependent UV–vis spectra were measured by a Cary 5000 UV–vis–NIR spectrophotometer with a temperature range from 25 to 100 °C. Solution absorption data was acquired from dilute solutions of polymers (0.05 mg/mL in *o*-DCB).

Photoluminescence Spectroscopy. Temperature-dependent steady-state photoluminescence measurements were recorded using a PTI-Horiba QuantaMaster 400 spectrofluorimeter equipped with a 75 W Xe arc lamp from 25 to 70 °C. The solution (0.05 mg/mL in *o*-DCB) was in a 10 mm quartz cuvette, which was stabilized at the desired temperature before measurement using an intercooler.

Small-Angle Neutron Scattering (SANS). SANS measurements were performed on dilute solutions of polymer (5 mg/mL) in *o*-DCB-*d*₄ to characterize the aggregate structure and single-chain conformation. The samples were measured in Hellma quartz cells with a 2 mm path length. Measurements were performed at the Extended Q-Range Small-Angle Neutron Scattering Diffractometer (EQ-SANS) at the Spallation Neutron Source (SNS), Oak Ridge National Lab (ORNL).³⁷ Two configurations (4 m sample to detector distance with a wavelength band of $\lambda_{min} = 12$ Å and 2.5 m sample to detector distance with $\lambda_{min} = 2.5$ Å) were used to cover the scattering wavevector q from 0.003 to 0.7 Å^{−1}. SANS measurements were performed at 25, 75, 100, and 130 °C for samples dissolved in *o*-DCB-*d*₄ solution. Scattering data were reduced and corrected by subtracting the background from solvents and cells. The data were put on an absolute scale (cm^{−1}) by using a standard porous silica sample.³⁸

Atomic Force Microscope (AFM). AFM images were acquired on an Asylum Research Cypher S AFM in tapping mode. Aged polymer solution (0.1 mg/mL in *o*-DCB, at room temperature for 24 h) was spin-coated onto the oxygen plasma cleaned silicon wafer at 600 rpm for 3 min and dried naturally before AFM measurements.

Transmission Electron Microscopy (TEM). TEM experiments were performed at 80 kV in a JEOL NEOARM at the Center for Nanophase Materials Sciences, Oak Ridge National Laboratory, which is using a cold field-emission gun with a typical emission current of 14–15 μA. Images were collected with mitigated electron beam exposure to reduce beam-induced sample changes. The samples were prepared by drop-casting the aged solution (0.1 mg/mL in *o*-DCB, at room temperature for 24 h) on 400 mesh copper grids.

Nuclear Magnetic Resonance (NMR). Temperature-dependent ¹H NMR spectra were measured by a Varian-500 MHz NMR spectrometer from 25 to 100 °C. D1 was set to be 5. Chemical shifts

were reported in ppm relative to *o*-DCB-*d*₄ at 7.17 ppm (lower field peak) for ¹H NMR.

Dynamic Light Scattering (DLS). The time-averaged scattering intensity was collected at a 90-deg angle for more than 2 min from a Brookhaven Instruments BI-200SM goniometer with an avalanche photodiode detector and TurboCorr correlator. DLS measurements were collected using a 633 nm HeNe laser from Research Electro Optics. The concentration of PffBT4T-based polymer solution used here was 0.1 mg/mL in *o*-DCB solvent. Variable-temperature solution DLS was measured from 25 to 70 °C.

RESULTS AND DISCUSSION

Physical Properties of PffBT4T-Based Polymers. Two PffBT4T polymers with different side chain lengths were considered here. Both polymers have high thermal stability, with thermal degradation temperatures exceeding 400 °C (Figure S1). The molecular weights (M_n), dispersity (D), and both melting and crystallization temperatures of both polymers were listed in Table 1. The M_n and D values for both polymers

Table 1. Basic Physical Properties of PffBT4T-Based Polymers

polymer name	M_n (kDa)	D	T_m (°C)	T_c (°C)
PffBT4T-C8C12	52.7	1.9	280.1	244.3
PffBT4T-C9C13	46.7	2.2	265.2	226.8

are close, thus allowing us to systematically compare their solution assembly behaviors. The sharp melting/crystallization peaks observed in DSC curves indicate the strong crystallization ability of both polymers. In addition, the PffBT4T polymer with longer side chains showed a 15–18 °C drop in both melting and crystallization temperatures. The DSC curves were shown in Figure S2.

Temperature-Dependent Solution Structure. Understanding the solution assembly of CPs has relied on a wide range of techniques, including spectroscopic analyses (e.g., UV-vis absorption and photoluminescence, PL), SANS,^{15,39} small-angle X-ray scattering (SAXS), static light scattering (LS),^{40,41} DLS,^{42–45} and viscometry.^{46,47} Optical spectroscopic analyses are powerful tools to identify the formation of aggregates. In *o*-DCB, at low temperature, PffBT4T polymers formed aggregates, given that the absorption profile presented distinct spectral features (0–1 and 0–0 transitions shown in Figure S3) due to intrachain and interchain order.^{35,48} The thermochromic blue shift in the absorption spectra upon increasing temperature was observed. When solution temperature raised from 25 to 100 °C, the sharp 0–0 transition peak at around 700 nm, which is due to polymer aggregation, reduced gradually and finally disappeared. This indicates that the polymer chains fully disaggregate, hence resulting in a featureless single absorption peak appearing near 550 nm. Furthermore, we measured temperature-dependent photoluminescence (PL) spectra of the solution (Figure S4, parts a and b) to explore the temperature-dependent aggregation behavior of the polymers. It is clear that when the solution of the polymer was heated from 25 to 70 °C, the PL emission peak shifted from 750 to 650 nm, while the intensity of the emission increased distinctly, indicating a gradual disaggregation process. At low temperatures (25 to 50 °C), the single-chain polymer fluorescence (650 nm) is significantly quenched, due to the efficient interchain interactions in aggregates. Despite being highly useful for understanding the optical property, the optical spectroscopic analyses provide

very limited structural information on the chain conformation of the assembled structure. In the following sections, we discuss our effort to correlate the solution structure and polymer's optoelectronic property.

Here, we reported the solution structure of the PffBT4T polymers using variable-temperature SANS, DLS, and NMR to rationalize the observed optical property at various temperatures. Solution SANS measurements with the schematic shown in Figure 1a were performed on PffBT4T-C8C12 and PffBT4T-C9C13 dissolved in *o*-DCB-*d*₄ solvent to characterize either a single chain conformation or aggregate structure. The concentration of the measured solution is 5 mg/mL, which is highly relevant to the ink used for processing final functional devices. The samples were initially fully dissolved in the *o*-DCB-*d*₄ solvent at 100 °C. Then the hot solutions were transferred to Hellma quartz cells with a 2 mm path length. After the solution cooled to room temperature, the sample in quartz cells formed a gel, and the solution was no longer able to flow before SANS measurements. In this case, as shown in parts c and d of Figure 1, the scattering signal from aggregates dominated the SANS profile, characterized by strong scattering intensity near the low scattering vector, which indicate that large structures, (e.g., >100 nm) were formed. This agrees with the previous measurements for P3AT and DPP gel,^{30,49} as well as polyfluorene gel.⁵⁰

In order to further understand the aggregate structure, we performed transmission electron microscopy (TEM) and atomic force microscope (AFM) to observe the morphology of aggregates. As shown in TEM and AFM images in parts e and f of Figure 1, a loosely packed network was formed by stacking primary nanoribbon-like small aggregates with each other. The aggregates of PffBT4T-C9C13 showed a more connected network compared to PffBT4T-C8C12 aggregates. The width of the primary nanoribbon-like small aggregates is on the order of nanometers (see Figure S5 for statistical data). The average width for PffBT4T-C8C12 aggregates (24 nm) is lower than that of PffBT4T-C9C13 aggregates (35 nm). The length of the aggregates can not be accurately measured due to the continuous nature of interconnected structures. The best estimation of length for aggregates ranges from hundred nanometers to a few microns. Height profiles of the aggregates shown in parts e and f of Figure 1 indicate sheet-like aggregates formed, with only about 2–3 nm in thickness for both PffBT4T-C8C12 and PffBT4T-C9C13. It is worth noting that a weak peak at q around 0.25 Å⁻¹ showed up in the SANS curves, which corresponds well with the alkyl chain packing (100) peak when aggregates pack together.³⁵

Next, we further performed variable-temperature SANS to measure the single-chain conformation at the elevated measurement temperatures. This allows us to quantify the backbone rigidity for PffBT4T polymers. As seen in parts c and d of Figure 1, upon heating, the scattering intensity decreases sharply at the low q region, indicating the dissolution of large polymer aggregates. The scattering result showed a clear Guinier region at the low q range at high temperatures. It can be seen that the SANS curves measured at 75, 100, and 130 °C can be fitted nicely with a flexible cylinder model in SasView,^{22,51} which is a suitable model for semiflexible polymers with side chains like CPs. This model has been utilized to fit the SANS curves for P3AT, PTB7, and DPP-based polymers as well as many other CPs.^{22,52–54} From this model, one can extract chain conformation, such as contour length (l_c), l_p , and cylinder radius (R) (see inset in Figure 1b

for this model). Parameters obtained from data fitting using the flexible cylinder model were shown in Table 2. According

Table 2. Parameters Obtained from Fits to the SANS Data with the Flexible Cylinder Model^a

polymer	T (°C)	l_c (nm)	l_p (nm)	radius (nm)
PffBT4T-C8C12	75	85.1 ± 2.0	3.0 ± 0.1	0.94 ± 0.01
	100	61.4 ± 3.1	3.1 ± 0.1	0.94 ± 0.01
	130	63.7 ± 3.4	3.1 ± 0.1	0.90 ± 0.01
PffBT4T-C9C13	75	78.3 ± 2.0	3.3 ± 0.3	0.95 ± 0.01
	100	56.3 ± 1.6	3.4 ± 0.4	0.95 ± 0.02
	130	54.7 ± 1.9	3.4 ± 0.4	0.95 ± 0.01

^aRadius is the cylinder radius, l_p is the persistence length, and l_c is the contour length, and the dispersity for contour length is 1.

to the SANS results, PffBT4T-C8C12 and PffBT4T-C9C13 are relatively flexible with l_p at a value of about 3 nm, which is very close to the l_p value reported for P3HT.^{14,15} Planarization of the polymer backbone upon fluorination has been observed for several polymers, such as regioregular poly(3-alkyl-4-fluoro)thiophenes,⁵⁵ indacenodithiophene-*co*-(difluorinated) benzothiadiazole (BT) polymer,⁵⁶ and DPP-based polymers.⁵⁷ This planarization is promoted by noncovalent interactions (H–F, S–F).⁵⁵ As calculated from the freely rotating chain model, PffBT4T-C8C12 is very rigid with a l_p of 13.3 nm.³⁴ Also, a recent atomistic molecular dynamics simulation work to probe the chain conformation indicated a high l_p of 7.1 nm for PffBT4T-C8C12.⁵⁸ Our experimental finding showed different results. At high temperatures, the interaction between the sulfur atom and fluorine atom is not strong enough to lock the chain conformation, thus resulting in a flexible backbone, as the thiophene majority building blocks dominate the chain

conformation. Thus, previously mentioned freely rotating chain model and atomistic molecular dynamics simulation could overestimate chain rigidity of PffBT4T-C8C12. This points to the need for better models and simulation protocols to calculate the chain rigidity of CPs.

Moreover, PffBT4T-C9C13 with a longer side chain shows a slightly higher value of l_p , at 3.4 nm versus 3.1 nm for PffBT4T-C8C12. However, a larger error bar in l_p value for PffBT4T-C9C13 is also observed. The stronger steric hindrance from longer side chains may slightly rigidify the polymer chain. Additionally, our results show that l_p for PffBT4T-C8C12 and PffBT4T-C9C13 is weakly dependent on temperature, with only slightly increased with increasing temperature (Figure 1b). The higher l_p at 75 °C than 100 and 130 °C indicates that aggregates containing dimer could persist at 75 °C. The dependence of l_p for CPs on temperature remains controversial. Segalman et al. reported that the measured l_p decrease as the temperature is increased for P3ATs due to a more twisted backbone.¹⁵ In Schneider and co-workers' recent work, they observed an increased chain rigidity of P3HT with rising temperature.⁵⁹ Overall, the variable-temperature SANS work showed the assembled structure from PffBT4T polymers is highly dependent on temperature, and it spans from multichain aggregates to a single flexible chain.

Aggregate Structure by DLS. According to the above discussion, polymer chains formed large aggregates below the aggregation-to-dissolved transition temperature. Here, to investigate the structure of the aggregates in the solution, variable-temperature DLS was also used. DLS measures the diffusion coefficient of aggregates in the solution, which in combination with the solution viscosity and the Stokes–Einstein equation gives the typical size (hydrodynamic radius, R_h) of aggregates. DLS has been used to probe the aggregation

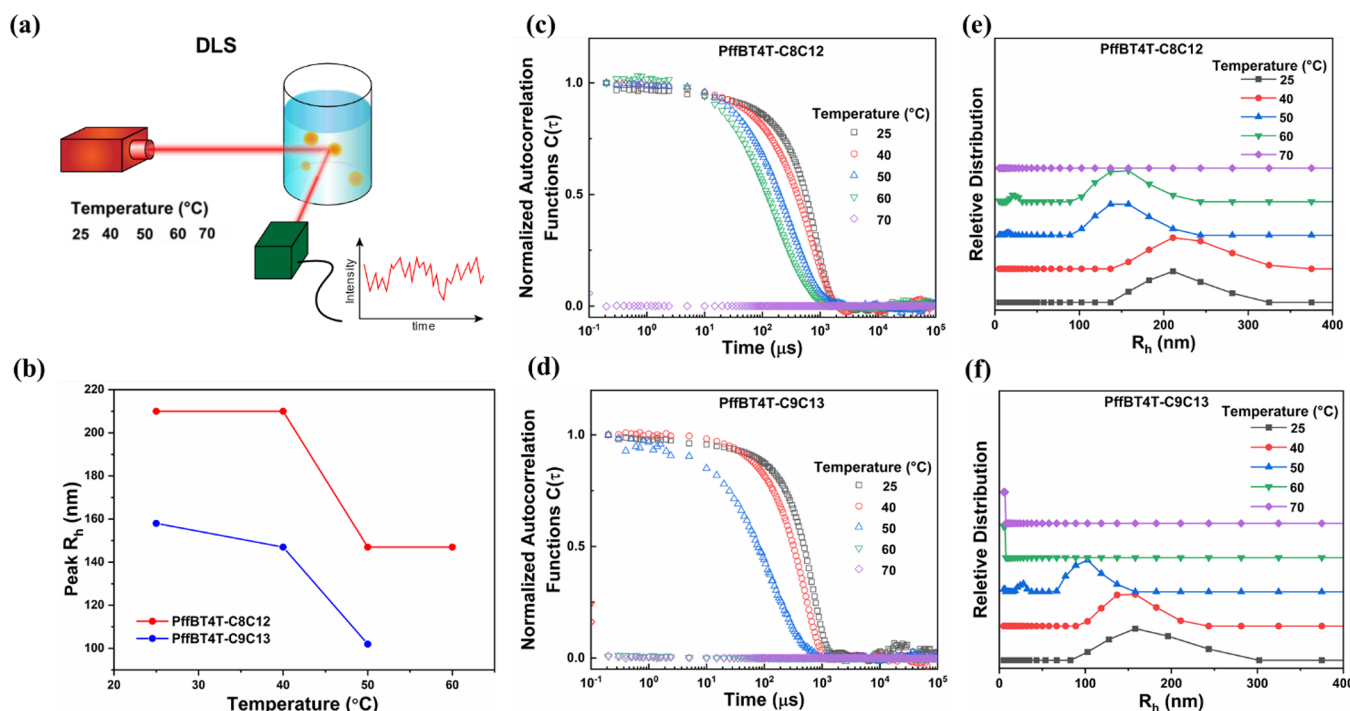


Figure 2. DLS to probe solution property for PffBT4T polymers. (a) Schematic of solution DLS. (b) Temperature dependence of the peak R_h in solution. (c and d) Temperature dependence of the normalized autocorrelation function. (e and f) Corresponding distribution of R_h . Polymer solution (0.1 mg/mL in *o*-DCB) was stored at room temperature for 24 h to promote aggregates at room temperature. The aggregated polymer solution was then heated to various temperatures and measured.

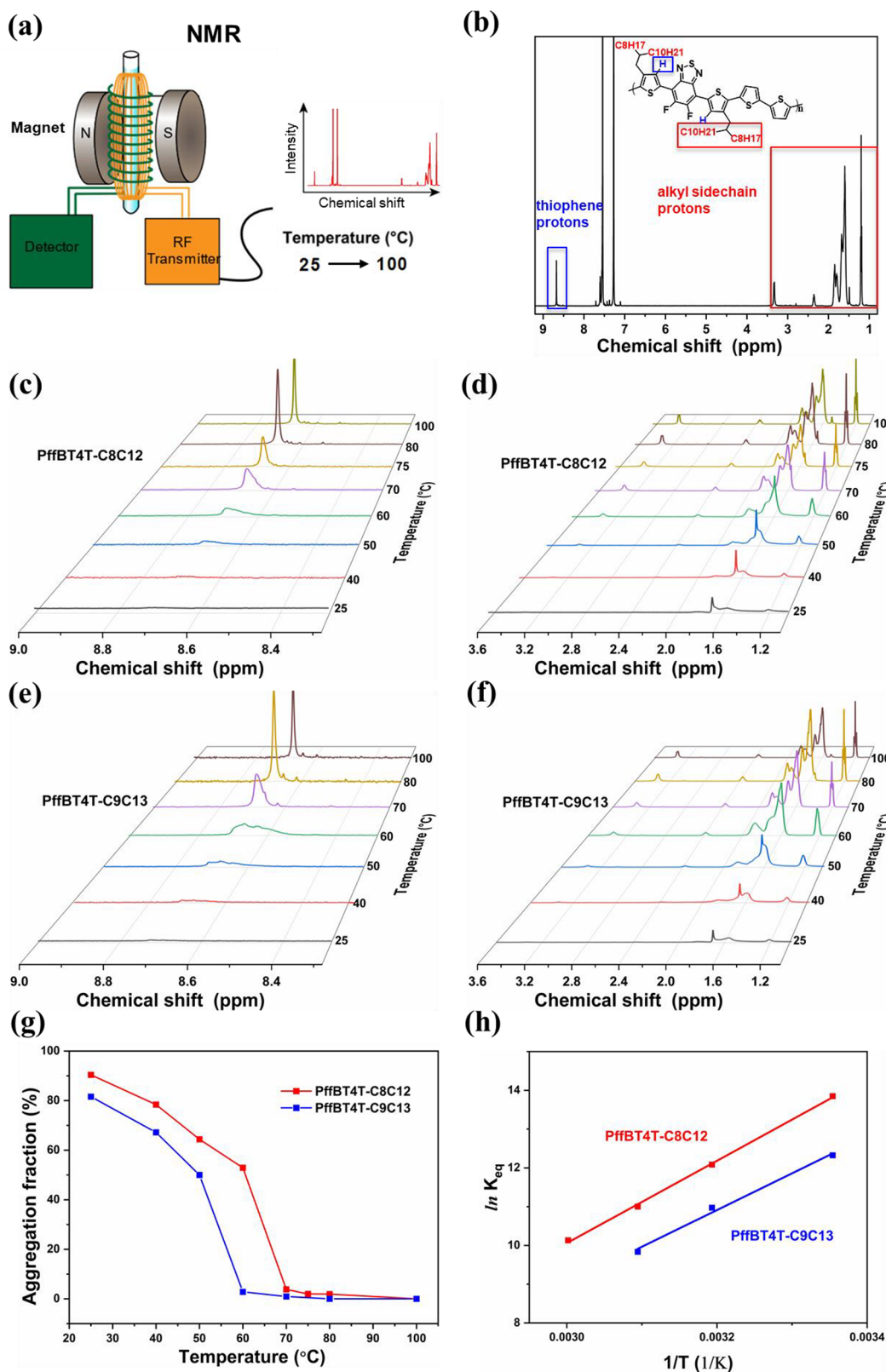


Figure 3. NMR to probe solution property for PffBT4T polymers at a concentration of 5 mg/mL in *o*-DCB- d_4 for different temperatures. (a) Schematic of NMR. (b) NMR spectra of PffBT4T-C8C12 measured at 100 °C. Temperature dependence of NMR aromatic peak of (c) PffBT4T-C8C12 and (d) of PffBT4T-C9C13. Temperature dependence of NMR alkyl peaks of (e) PffBT4T-C8C12 and (f) PffBT4T-C9C13. (g) Aggregation fraction of PffBT4T-C8C12 and PffBT4T-C9C13. The degree of aggregation was calculated by comparing the peak areas of alkyl peaks with the peak areas of fully dissolved polymers at 100 °C. (h) Van't Hoff plot for the temperature dependence of the dimerization constant of PffBT4T-C8C12 and PffBT4T-C9C13.

behavior of polythiophenes,⁶⁰ polyphenylenevinylenes,⁶¹ poly(9,9-diptylfluorene),⁵⁰ and DPP-based polymers,²³ but it remains underutilized for PffBT4T-based polymers. Since the DLS only concerns temporal fluctuations for PffBT4T-based polymer aggregates within the illustrated beam path, the weak absorption from the dilute solution will not affect the R_h value.

To study the structure of primary aggregates at different temperatures, we performed variable-temperature DLS (Figure 2a) to observe the disaggregation process by heating preaggregated dilute solution (0.1 mg/mL in *o*-DCB) that was previously aged at room temperature for 24 h. At low temperatures, the relaxation time of polymer aggregates in solution is around 1 ms which agrees with the expected diffusion behavior for large aggregates (100–300 nm). The relaxation time of the solution gradually reduced with the temperature raised for both PffBT4T-C8C12 (Figure 2c) and PffBT4T-C9C13 (Figure 2d). The corresponding R_h of aggregates with increasing temperature is shown in Figure 2, parts e and f. As can be seen in Figure 2b, the most plausible R_h decreases gradually from ~210 to ~130 nm during the heating for PffBT4T-C8C12 and from ~160 to ~100 nm for PffBT4T-C9C13 from room temperature to 60 °C. At 70 °C, no large aggregates were observed by DLS for PffBT4T-C8C12, indicating that the aggregates were fully disaggregated. For PffBT4T-C9C13, no large size aggregates were observed at a lower temperature of 60 °C. Apart from the aggregation-to-dissolved chain transition temperature, it is worth noting that the size of alkyl chains also influences the size of the aggregates in solution. The size of the aggregates of PffBT4T-C8C12 was bigger than PffBT4T-C9C13 at the same temperature, indicating the longer side chain hinders the further growth of aggregates in solution.

Degree of Aggregation by NMR in Solutions. At present, the lack of simple characterization methods to characterize the degree of aggregation of CPs in solution at high concentration (e.g., a few mg/mL) pertained to the device manufacture limited the understanding on their aggregation behavior. Optical spectroscopic analyses were commonly used to study the degree of aggregation in very dilute solutions (<0.1 mg/mL). Scattering measurements need a complex model to decouple the signal originating from the aggregates and single chains, which is prone to error since large structures dominate the scattering signal.²⁹ Thus, careful consideration should be given when modeling the scattering data. A good example is from Pozzo group to measure samples at a wide range of scattering vectors, combining ultrasmall-angle neutron scattering with small-angle neutron scattering and applying the appropriate model.²²

In this section, we studied the aggregation behavior of PffBT4T-based polymers in solution (5 mg/mL) by NMR, which is sensitive to the local electronic environment of an atom with nonzero nuclear spin. Figure 3a shows the schematic of NMR. Once they form aggregates, the protons in aggregates will not contribute strongly to the NMR spectra due to the shielding effect and slow chain dynamics. Figure 3b shows the ^1H NMR spectra of PffBT4T-C8C12 in *o*-DCB-*d*₄ at 100 °C. The chemical shifts of protons from the thiophene rings (8.6–8.8 ppm) and alkyl side chains (1.1–3.6 ppm) were observed clearly at such high temperatures indicating a fully dissolved single chain in solution. As shown in parts c and e of Figure 3, nevertheless, no aromatic peak was observed at room temperature for PffBT4T-C8C12 and PffBT4T-C9C13, indicating the formation of aggregates as π – π stacking in

aggregates leads to shielding.⁶² Furthermore, parts d and f of Figure 3 show that the alkyl peaks also almost disappear at room temperature, which is indicative of the existence of interaction between alkyl side chains in aggregates. With the increase of temperature, the NMR spectrum peaks gradually appeared and narrowed from broad peaks.

We also calculated the aggregation fraction at different temperatures by comparing the peak areas of alkyl peaks with peak areas of fully dissolved polymers at 100 °C. As can be seen in Figure 3g, at room temperature, most molecular chains (90% for PffBT4T-C8C12 and 80% PffBT4T-C9C13) are in aggregated states. Most of the sample precipitates out as can also be seen with the naked eye (Figure S7). Similarly, the UV–vis spectroscopy results also showed a high aggregation fraction at room temperature. By calculating the relative peak area of single-chain absorption peak (from the multiplet fitting of the absorption spectra, normalized to 80 °C) as a function of temperature, we compare the degree of aggregation of PffBT4T-C8C12 and PffBT4T-C9C13 solutions at various temperatures, as shown in Figure S3c. Over 80% of the chains are in the aggregated state even in dilute solution (e.g., 0.05 mg/mL) at room temperature. Note that more pronounced disaggregation with increasing temperature was observed in such a more dilute solution. In addition to the solution temperature, the degree of aggregation is also affected by the side chain length. PffBT4T-C8C12 with a shorter side chain showed a higher aggregation fraction at the same temperature and higher onset temperature (60 °C for PffBT4T-C9C13, and 70 °C for PffBT4T-C9C13) to be fully dissolved compared with PffBT4T-C9C13, suggesting that the longer side chain could induce less thermally stable aggregates due to stronger steric hindrance.

Thermodynamics and Kinetics of Aggregation.

Despite the importance of the aggregation behavior of CPs, the fundamental thermodynamics features during aggregation have rarely been studied before, which is pivotal for the precise control of the self-assembly process.⁶³ In solution, aggregation of CPs can be considered as the thermodynamic equilibrium between single-chain species and aggregate species. The abundant aggregate species lead to multiple equilibria in the solution. Assuming an isodesmic aggregation behavior and for the sake of simplicity, we used a simplified monomer–dimer model to describe the equilibrium for the aggregation process. Similar models were widely applied to the aggregation of dye molecules such as cyanine⁶⁴ and phthalocyanine dyes⁶⁵ and more recently for dipolar merocyanine dyes.⁶⁶ The simple dimerization model can be expressed as

$$K_{\text{dim}} = \frac{C_D}{C_M^2} \quad (1)$$

where K_{dim} denotes the dimerization constant for $\text{M} + \text{M} \rightleftharpoons \text{D}$ and C_M and C_D are the concentrations of monomer and dimer. The standard aggregation enthalpy change and entropy change of dimerization of the PffBT4T-C8C12 and PffBT4T-C9C13 in *o*-DCB-*d*₄ were obtained by means of a Van't Hoff plot according to temperature-dependent NMR experiments, where the K_{dim} values were determined at variable temperatures.

$$\ln K_{\text{dim}} = -\frac{\Delta H^\circ}{RT} + \frac{\Delta S^\circ}{R} \quad (2)$$

The plot of $\ln K_{\text{dim}}$ versus $1/T$ can be fitted by a linear relationship (Figure 3h). The standard dimerization enthalpy

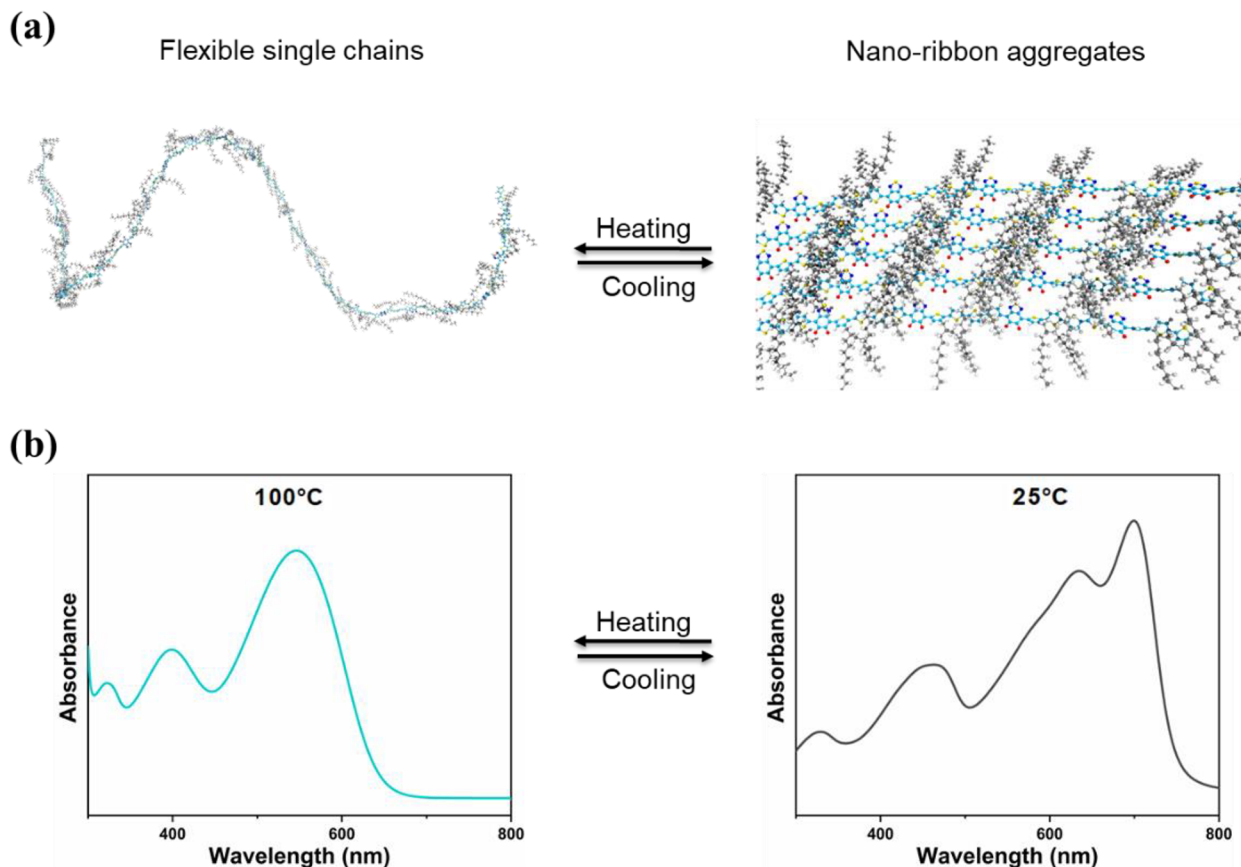


Figure 4. (a) Schematic of temperature-dependent solution structure of PffBT4T polymers. (b) Temperature-dependent UV-vis of PffBT4T polymers.

and entropy were determined to be $\Delta H^\circ = -88.3 \pm 3.9 \text{ kJ mol}^{-1}$ and $\Delta S^\circ = -181.2 \pm 12.5 \text{ J mol}^{-1} \text{ K}^{-1}$ for PffBT4T-C8C12 and $\Delta H^\circ = -78.8 \pm 6.9 \text{ kJ mol}^{-1}$ and $\Delta S^\circ = -161.4 \pm 22.2 \text{ J mol}^{-1} \text{ K}^{-1}$ for PffBT4T-C9C13. These data suggest that the aggregation is enthalpically driven. The polymer with the longer side chain has a greater enthalpy of solvation that is lost upon forming a dimer. This explains the less enthalpy gain of PffBT4T-C9C13. The smaller entropy penalty seen on PffBT4T-C9C13 during aggregation is likely due to the lower degree of enthalpy–entropy compensation as a result of the weaker aggregation enthalpy.

The kinetics of polymer aggregation for CPs plays a key role in influencing the film-forming dynamics. In previous studies, *in situ* grazing incidence wide-angle X-ray scattering (GIWAXS) has been used to investigate the PffBT4T-C8C12 aggregation pathway during the transformation from solution to dried films.⁶⁷ Aggregates could form within a few seconds. However, in the previous report, there is simultaneous rapid solvent evaporation and temperature drop, which makes it difficult to deconvolute various factors and study the effects of temperature on polymer aggregation alone. Here, we monitored the aggregation process of PffBT4T-based polymers during cooling by NMR and UV-vis at constant polymer concentration. The polymers were initially fully dissolved in *o*-DCB-*d*₄ solvent at 100 °C and then cooled and aged at 25 °C. ¹H NMR spectra of PffBT4T-C8C12 and PffBT4T-C9C13 solution in *o*-DCB-*d*₄ at a concentration of 5 mg/mL were taken during the cooling and aging were shown in Figure S10. We observed that both aromatic peaks and alkyl peaks gradually disappeared and formed broad peaks. We further

calculated the aggregation fraction at different times. Our data indicated that most aggregates formed within the first 3 min for PffBT4T-C8C12, or within 5 min for PffBT4T-C9C13, and then aggregate formation slowed down. It is clear that the aggregation process exhibited an S-like curve, representing the continuous nucleation and growth stage. Similar results were also observed in cooling experiments for both PffBT4T-C8C12 and PffBT4T-C9C13 solution by UV-vis. By monitoring the absorption peak tied to chain aggregates at 700 nm during *in situ* aging at 25 °C at a concentration of 0.05 mg/mL, we found that within the first 5 min for PffBT4T-C8C12 and 10 min for PffBT4T-C9C13 most of the aggregates formed (see Figure S11).

We have found a strongly temperature-dependent solution structure for PffBT4T polymers. Fully dissolved PffBT4T polymer chains are relatively flexible with l_p at a value of about 3 nm. The relatively flexible single chains can explain the obvious blue shift once fully dissolved. Even though we cannot measure the conformation of the polymer chains in the aggregate, a more planar and rigid backbone conformation is expected owing to the constraints of the surrounding molecular chains (as shown in Figure 4a), based on the existing morphology characterization results, especially the finding from the TEM and alkyl chain stacking peak from the SANS results.^{68,69} The conformational change of the molecular chain results in a significant red shift in optical absorption, as can be seen in Figure 4b.

CONCLUSIONS

The solution structures of PffBT4T-C8C12 and PffBT4T-C9C13 were measured using variable-temperature UV-vis, DLS, NMR, and SANS tools. Fine-tuning the size of alkyl chains is particularly important to control the solution structure as well as the thermodynamics of aggregation. PffBT4T-C8C12 shows a stronger aggregation tendency than PffBT4T-C9C13 due to less steric hindrance from side chains, as indicated by more thermally stable aggregates, the higher degree of aggregation, more aggregation enthalpy gain, and the larger size of the aggregates in solution. PffBT4T-C8C12 shows a slightly lower l_p than PffBT4T-C9C13, and both polymers are relatively flexible with l_p at a value of about 3 nm, which remains nearly constant with increasing temperature once above the disaggregation temperature around 75 °C. This work indicated the solution structure can be dramatically tuned by slightly varying the alkyl side chain length which can be taken advantage of to achieve ideal morphology for high-performance optoelectronics applications.

ASSOCIATED CONTENT

Supporting Information

The Supporting Information is available free of charge at <https://pubs.acs.org/doi/10.1021/acsapm.1c01511>.

TGA, DSC, UV-vis, PL, and NMR results (PDF)

AUTHOR INFORMATION

Corresponding Author

Xiaodan Gu — *School of Polymer Science and Engineering, The University of Southern Mississippi, Hattiesburg, Mississippi 39406, United States;  orcid.org/0000-0002-1123-3673; Email: xiaodan.gu@usm.edu*

Authors

Zhiqiang Cao — *School of Polymer Science and Engineering, The University of Southern Mississippi, Hattiesburg, Mississippi 39406, United States*

Guorong Ma — *School of Polymer Science and Engineering, The University of Southern Mississippi, Hattiesburg, Mississippi 39406, United States*

Mingwan Leng — *Department of Chemistry, Texas A&M University, College Station, Texas 77843, United States*

Song Zhang — *School of Polymer Science and Engineering, The University of Southern Mississippi, Hattiesburg, Mississippi 39406, United States;  orcid.org/0000-0001-9815-7046*

Jihua Chen — *Center for Nanophase Materials Sciences, Oak Ridge National Laboratory, Oak Ridge, Tennessee 37831, United States*

Changwoo Do — *Neutron Scattering Division, Oak Ridge National Laboratory, Oak Ridge, Tennessee 37831, United States;  orcid.org/0000-0001-8358-8417*

Kunlun Hong — *Center for Nanophase Materials Sciences, Oak Ridge National Laboratory, Oak Ridge, Tennessee 37831, United States;  orcid.org/0000-0002-2852-5111*

Lei Fang — *Department of Chemistry, Texas A&M University, College Station, Texas 77843, United States;  orcid.org/0000-0003-4757-5664*

Complete contact information is available at:

<https://pubs.acs.org/doi/10.1021/acsapm.1c01511>

Notes

The authors declare no competing financial interest.

ACKNOWLEDGMENTS

This work was supported by the National Science Foundation (NSF) under Award Numbers CHE-2004133 and CHE-2003733. Part of the research used resources at the Spallation Neutron Source and the Center for Nanophase Materials Sciences (CNMS), DOE Office of Science User Facilities, operated by the Oak Ridge National Laboratory. TEM was conducted at the Center for Nanophase Materials Sciences, which is a DOE Office of Science User Facility. SANS measurements were carried out using the EQ-SANS at SNS, ORNL. The authors thank Peter V. Bonnesen (CNMS) for assistance during the NMR experiment.

REFERENCES

- (1) Zhao, J.; Li, Y.; Yang, G.; Jiang, K.; Lin, H.; Ade, H.; Ma, W.; Yan, H. Efficient Organic Solar Cells Processed from Hydrocarbon Solvents. *Nat. Energy* **2016**, *1* (2), 15027.
- (2) Cui, Y.; Wang, Y.; Bergqvist, J.; Yao, H.; Xu, Y.; Gao, B.; Yang, C.; Zhang, S.; Inganäs, O.; Gao, F.; Hou, J. Wide-Gap Non-Fullerene Acceptor Enabling High-Performance Organic Photovoltaic Cells for Indoor Applications. *Nat. Energy* **2019**, *4* (9), 768–775.
- (3) Nikolka, M.; Broch, K.; Armitage, J.; Hanifi, D.; Nowack, P. J.; Venkateshvaran, D.; Sadhanala, A.; Saska, J.; Mascal, M.; Jung, S. H.; Lee, J. K.; McCulloch, I.; Salleo, A.; Sirringhaus, H. High-Mobility, Trap-Free Charge Transport in Conjugated Polymer Diodes. *Nat. Commun.* **2019**, *10* (1), 1–9.
- (4) Wang, S.; Xu, J.; Wang, W.; Wang, G.-J. N.; Rastak, R.; Molina-Lopez, F.; Chung, J. W.; Niu, S.; Feig, V. R.; Lopez, J.; Lei, T.; Kwon, S.-K.; Kim, Y.; Foudeh, A. M.; Ehrlich, A.; Gasperini, A.; Yun, Y.; Murmann, B.; Tok, J. B.-H.; Bao, Z. Skin Electronics from Scalable Fabrication of an Intrinsically Stretchable Transistor Array. *Nature* **2018**, *555*, 83–88.
- (5) Nikolka, M.; Nasrallah, I.; Rose, B.; Ravva, M. K.; Broch, K.; Sadhanala, A.; Harkin, D.; Charmet, J.; Hurhangee, M.; Brown, A.; Illig, S.; Too, P.; Jongman, J.; McCulloch, I.; Bredas, J. L.; Sirringhaus, H. High Operational and Environmental Stability of High-Mobility Conjugated Polymer Field-Effect Transistors through the Use of Molecular Additives. *Nat. Mater.* **2017**, *16* (3), 356–362.
- (6) Ashizawa, M.; Zheng, Y.; Tran, H.; Bao, Z. Intrinsically Stretchable Conjugated Polymer Semiconductors in Field Effect Transistors. *Prog. Polym. Sci.* **2020**, *100*, 101181.
- (7) Ohayon, D.; Nikiforidis, G.; Savva, A.; Giugni, A.; Wustoni, S.; Palanisamy, T.; Chen, X.; Maria, I. P.; Di Fabrizio, E.; Costa, P. M. F. J.; McCulloch, I.; Inal, S. Biofuel Powered Glucose Detection in Bodily Fluids with an N-Type Conjugated Polymer. *Nat. Mater.* **2020**, *19* (4), 456–463.
- (8) London, A. E.; Chen, H.; Sabuj, M. A.; Tropp, J.; Saghayezhian, M.; Egedugurala, N.; Zhang, B. A.; et al. A High-Spin Ground-State Donor-Acceptor Conjugated Polymer. *Sci. Adv.* **2019**, *5*, eaav2336.
- (9) Zhan, L.; Li, S.; Xia, X.; Li, Y.; Lu, X.; Zuo, L.; Shi, M.; Chen, H. Layer-by-Layer Processed Ternary Organic Photovoltaics with Efficiency over 18%. *Adv. Mater.* **2021**, *33* (12), 2007231.
- (10) Wang, C.; Liu, F.; Chen, Q.-M.; Xiao, C.-Y.; Wu, Y.-G.; Li, W.-W. Benzothiadiazole-Based Conjugated Polymers for Organic Solar Cells. *Chin. J. Polym. Sci.* **2021**, *39* (5), 525–536.
- (11) Li, J.; Zhao, Y.; Tan, H. S.; Guo, Y.; Di, C.-A.; Yu, G.; Liu, Y.; Lin, M.; Lim, S. H.; Zhou, Y.; Su, H.; Ong, B. S. A Stable Solution-Processed Polymer Semiconductor with Record High-Mobility for Printed Transistors. *Sci. Rep.* **2012**, *2*, 754.
- (12) Gu, X.; Shaw, L.; Gu, K.; Toney, M. F.; Bao, Z. The Meniscus-Guided Deposition of Semiconducting Polymers. *Nat. Commun.* **2018**, *9* (1), 534.
- (13) Xu, Z.; Park, K. S.; Diao, Y. What Is the Assembly Pathway of a Conjugated Polymer From Solution to Thin Films? *Front. Chem.* **2020**, *8*, 583521.
- (14) Newbloom, G. M.; Hoffmann, S. M.; West, A. F.; Gile, M. C.; Sista, P.; Cheung, H. K. C.; Luscombe, C. K.; Pfaendtner, J.; Pozzo, L.

D. Solvatochromism and Conformational Changes in Fully Dissolved Poly(3-Alkylthiophene)S. *Langmuir* **2015**, *31* (1), 458–468.

(15) McCulloch, B.; Ho, V.; Hoarfrost, M.; Stanley, C.; Do, C.; Heller, W. T.; Segalman, R. A. Polymer Chain Shape of Poly(3-Alkylthiophenes) in Solution Using Small-Angle Neutron Scattering. *Macromolecules* **2013**, *46* (5), 1899–1907.

(16) Gettinger, C. L.; Heeger, A. J.; Drake, J. M.; Pine, D. J. A Photoluminescence Study of Poly(Phenylene Vinylene) Derivatives: The Effect of Intrinsic Persistence Length. *J. Chem. Phys.* **1994**, *101* (2), 1673–1678.

(17) Li, Y.-C.; Chen, C.-Y.; Chang, Y.-X.; Chuang, P.-Y.; Chen, J.-H.; Chen, H.-L.; Hsu, C.-S.; Ivanov, V. A.; Khalatur, P. G.; Chen, S.-A. Scattering Study of the Conformational Structure and Aggregation Behavior of a Conjugated Polymer Solution. *Langmuir* **2009**, *25* (8), 4668–4677.

(18) Lukyanov, A.; Malafeev, A.; Ivanov, V.; Chen, H. L.; Kremer, K.; Andrienko, D. Solvated Poly-(Phenylene Vinylene) Derivatives: Conformational Structure and Aggregation Behavior. *J. Mater. Chem.* **2010**, *20* (46), 10475–10485.

(19) Fytas, G.; Nothofer, H. G.; Scherf, U.; Vlassopoulos, D.; Meier, G. Structure and Dynamics of Nondilute Polyfluorene Solutions. *Macromolecules* **2002**, *35* (2), 481–488.

(20) Knaapila, M.; Stepanyan, R.; Torkkeli, M.; Lyons, B. P.; Ikonen, T. P.; Almásy, L.; Foreman, J. P.; Serimaa, R.; Güntner, R.; Scherf, U.; Monkman, A. P. Influence of Molecular Weight on the Phase Behavior and Structure Formation of Branched Side-Chain Hairy-Rod Polyfluorene in Bulk Phase. *Phys. Rev. E* **2005**, *71* (4), 41802.

(21) Kuei, B.; Gomez, E. D. Chain Conformations and Phase Behavior of Conjugated Polymers. *Soft Matter* **2017**, *13* (1), 49–67.

(22) Reid, D. R.; Jackson, N. E.; Bourque, A. J.; Snyder, C. R.; Jones, R. L.; de Pablo, J. J. Aggregation and Solubility of a Model Conjugated Donor–Acceptor Polymer. *J. Phys. Chem. Lett.* **2018**, *9* (16), 4802–4807.

(23) Liu, C.; Hu, W.; Jiang, H.; Liu, G.; Han, C. C.; Siringhaus, H.; Boué, F.; Wang, D. Chain Conformation and Aggregation Structure Formation of a High Charge Mobility DPP-Based Donor–Acceptor Conjugated Polymer. *Macromolecules* **2020**, *53* (19), 8255–8266.

(24) Xi, Y.; Wolf, C. M.; Pozzo, L. D. Self-Assembly of Donor–Acceptor Conjugated Polymers Induced by Miscible ‘poor’ Solvents. *Soft Matter* **2019**, *15* (8), 1799–1812.

(25) Zheng, Y. Q.; Yao, Z. F.; Lei, T.; Dou, J. H.; Yang, C. Y.; Zou, L.; Meng, X.; Ma, W.; Wang, J. Y.; Pei, J. Unraveling the Solution-State Supramolecular Structures of Donor–Acceptor Polymers and Their Influence on Solid-State Morphology and Charge-Transport Properties. *Adv. Mater.* **2017**, *29* (42), 1701072.

(26) Wang, Z.-Y.; Yao, Z.-F.; Lu, Y.; Ding, L.; Yu, Z.-D.; You, H.-Y.; Wang, X.-Y.; Zhou, Y.-Y.; Zou, L.; Wang, J.-Y.; Pei, J. Precise Tracking and Modulating Aggregation Structures of Conjugated Copolymers in Solutions. *Polym. Chem.* **2020**, *11* (22), 3716–3722.

(27) Chu, P. H.; Kleinhenz, N.; Persson, N.; McBride, M.; Hernandez, J. L.; Fu, B.; Zhang, G.; Reichmanis, E. Toward Precision Control of Nanofiber Orientation in Conjugated Polymer Thin Films: Impact on Charge Transport. *Chem. Mater.* **2016**, *28* (24), 9099–9109.

(28) Newbloom, G. M.; Weigandt, K. M.; Pozzo, D. C. Structure and Property Development of Poly(3-Hexylthiophene) Organogels Probed with Combined Rheology, Conductivity and Small Angle Neutron Scattering. *Soft Matter* **2012**, *8* (34), 8854–8864.

(29) Newbloom, G. M.; de la Iglesia, P.; Pozzo, L. D. Controlled Gelation of Poly(3-Alkylthiophene)s in Bulk and in Thin-Films Using Low Volatility Solvent/Poor-Solvent Mixtures. *Soft Matter* **2014**, *10* (44), 8945–8954.

(30) Xi, Y.; Li, D. S.; Newbloom, G. M.; Tatum, W. K.; O’Donnell, M.; Luscombe, C. K.; Pozzo, L. D. Sonocrystallization of Conjugated Polymers with Ultrasound Fields. *Soft Matter* **2018**, *14* (24), 4963–4976.

(31) Knaapila, M.; Dias, F. B.; Garamus, V. M.; Almásy, L.; Torkkeli, M.; Leppänen, K.; Galbrecht, F.; Preis, E.; Burrows, H. D.; Scherf, U.; Monkman, A. P. Influence of Side Chain Length on the Self-Assembly of Hairy-Rod Poly(9,9-Dialkylfluorene)s in the Poor Solvent Methylcyclohexane. *Macromolecules* **2007**, *40* (26), 9398–9405.

(32) Chen, C.; Chan, S.; Li, J.; Wu, K.; Chen, H.; Chen, J.; Huang, W.; Chen, S. Formation and Thermally-Induced Disruption of Nanowhiskers in Poly (3-Hexylthiophene)/ Xylene Gel Studied by Small-Angle X-Ray Scattering. *Macromolecules* **2010**, *43* (17), 7305–7311.

(33) Noriega, R.; Rivnay, J.; Vandewal, K.; Koch, F. P. V.; Stingelin, N.; Smith, P.; Toney, M. F.; Salleo, A. A General Relationship between Disorder, Aggregation and Charge Transport in Conjugated Polymers. *Nat. Mater.* **2013**, *12* (11), 1038–1044.

(34) Kuei, B.; Gomez, E. D. Chain Conformations and Phase Behavior of Conjugated Polymers. *Soft Matter* **2017**, *13* (1), 49–67.

(35) Liu, Y.; Zhao, J.; Li, Z.; Mu, C.; Ma, W.; Hu, H.; Jiang, K.; Lin, H.; Ade, H.; Yan, H. Aggregation and Morphology Control Enables Multiple Cases of High-Efficiency Polymer Solar Cells. *Nat. Commun.* **2014**, *5* (9), 1–8.

(36) Yao, H.; Li, Y.; Hu, H.; Chow, P. C. Y.; Chen, S.; Zhao, J.; Li, Z.; Carpenter, J. H.; Lai, J. Y. L.; Yang, G.; Liu, Y.; Lin, H.; Ade, H.; Yan, H. A Facile Method to Fine-Tune Polymer Aggregation Properties and Blend Morphology of Polymer Solar Cells Using Donor Polymers with Randomly Distributed Alkyl Chains. *Adv. Energy Mater.* **2018**, *8* (6), 1701895.

(37) Zhao, J. K.; Gao, C. Y.; Liu, D. The Extended Q-Range Small-Angle Neutron Scattering Diffractometer at the SNS. *J. Appl. Crystallogr.* **2010**, *43* (5), 1068–1077.

(38) Heller, W. T.; Cuneo, M.; Debeer-Schmitt, L.; Do, C.; He, L.; Heroux, L.; Littrell, K.; Pingali, S. V.; Qian, S.; Stanley, C.; Urban, V. S.; Wu, B.; Bras, W. The Suite of Small-Angle Neutron Scattering Instruments at Oak Ridge National Laboratory. *J. Appl. Crystallogr.* **2018**, *51* (2), 242–248.

(39) Aime, J. P.; Bargain, F.; Schott, M.; Eckhardt, H.; Miller, G. G.; Elsenbaumer, R. L. Structural Study of Doped and Undoped Polythiophene in Solution by Small-Angle Neutron Scattering. *Phys. Rev. Lett.* **1989**, *62* (1), 55–58.

(40) Zhao, L.-H.; Png, R.-Q.; Zhuo, J.-M.; Wong, L.-Y.; Tang, J.-C.; Su, Y.-S.; Chua, L.-L. Role of Borderline Solvents to Induce Pronounced Extended-Chain Lamellar Order in π -Stackable Polymers. *Macromolecules* **2011**, *44* (24), 9692–9702.

(41) Fytas, G.; Nothofer, H. G.; Scherf, U.; Vlassopoulos, D.; Meier, G. Structure and Dynamics of Nondilute Polyfluorene Solutions. *Macromolecules* **2002**, *35* (2), 481–488.

(42) Baun, A.; Wang, Z.; Morsbach, S.; Qiu, Z.; Narita, A.; Fytas, G.; Müllen, K. Rigidification of Poly(p-Phenylene)s through Ortho-Phenyl Substitution. *Macromolecules* **2020**, *53* (14), 5756–5762.

(43) Somma, E.; Loppinet, B.; Fytas, G.; Setayesh, S.; Jacob, J.; Grimsdale, A. C.; Müllen, K. Collective Orientation Dynamics in Semi-Rigid Polymers. *Colloid Polym. Sci.* **2004**, *282* (8), 867–873.

(44) Petekidis, G.; Fytas, G.; Scherf, U.; Müllen, K.; Fleischer, G. Dynamics of Poly(p-Phenylene) Ladder Polymers in Solution. *J. Polym. Sci., Part B: Polym. Phys.* **1999**, *37* (16), 2211–2220.

(45) Petekidis, G.; Vlassopoulos, D.; Fytas, G.; Rüklens, R.; Wegner, G. Orientation Dynamics and Correlations in Hairy-Rod Polymers: Concentrated Regime. *Macromolecules* **1998**, *31* (18), 6129–6138.

(46) Heffner, G. W.; Pearson, D. S. Molecular Characterization of Poly(3-Hexylthiophene). *Macromolecules* **1991**, *24* (23), 6295–6299.

(47) Bi, X.; Ying, Q.; Qian, R. Intrinsic Viscosity versus Molar Mass Relationship of Poly(3-Hexylthiophene) in Toluene. *Die Makromol. Chemie* **1992**, *193* (11), 2905–2914.

(48) Ma, W.; Yang, G.; Jiang, K.; Carpenter, J. H.; Wu, Y.; Meng, X.; et al. Influence of Processing Parameters and Molecular Weight on the Morphology and Properties of High-Performance PffBT4T-2OD : PC 71 BM Organic Solar Cells. *Adv. Energy Mater.* **2015**, *5* (23), 1501400.

(49) Newbloom, G. M.; Weigandt, K. M.; Pozzo, D. C. Electrical, Mechanical, and Structural Characterization of Self-Assembly in Poly(3-Hexylthiophene) Organogel Networks. *Macromolecules* **2012**, *45* (8), 3452–3462.

(50) Chen, J. H.; Chang, C. S.; Chang, Y. X.; Chen, C. Y.; Chen, H. L.; Chen, S. A. Gelation and Its Effect on the Photophysical Behavior of Poly(9, 9-Dioctylfluorene-2, 7-Diyi) in Toluene. *Macromolecules* **2009**, *42* (4), 1306–1314.

(51) This work benefited from the use of the SasView application, originally developed under NSF Award DMR-0520547. SasView contains code developed with funding from the European Union's Horizon 2020 Research and Innovation Programme under SINE20. www.sasview.org/.

(52) Cao, Z.; Li, Z.; Zhang, S.; Galuska, L.; Li, T.; Do, C.; Xia, W.; Hong, K.; Gu, X. Decoupling Poly(3-Alkylthiophenes)' Backbone and Side-Chain Conformation by Selective Deuteration and Neutron Scattering. *Macromolecules* **2020**, *53* (24), 11142–11152.

(53) Ocheje, M. U.; Goodman, R. B.; Lu, K.-T.; Wang, Y.; Galuska, L. A.; Soullard, L.; Cao, Z.; Zhang, S.; Yadiki, M.; Gu, X.; Chiu, Y.-C.; Rondeau-Gagné, S. Precise Control of Noncovalent Interactions in Semiconducting Polymers for High-Performance Organic Field-Effect Transistors. *Chem. Mater.* **2021**, *33* (21), 8267–8277.

(54) Galuska, L. A.; McNutt, W. W.; Qian, Z.; Zhang, S.; Weller, D. W.; Dhakal, S.; King, E. R.; Morgan, S. E.; Azoulay, J. D.; Mei, J.; Gu, X. Impact of Backbone Rigidity on the Thermomechanical Properties of Semiconducting Polymers with Conjugation Break Spacers. *Macromolecules* **2020**, *53* (14), 6032–6042.

(55) Fei, Z.; Boufflet, P.; Wood, S.; Wade, J.; Moriarty, J.; Gann, E.; Ratcliff, E. L.; McNeill, C. R.; Sirringhaus, H.; Kim, J. S.; Heeney, M. Influence of Backbone Fluorination in Regioregular Poly(3-Alkyl-4-Fluoro)Thiophenes. *J. Am. Chem. Soc.* **2015**, *137* (21), 6866–6879.

(56) Wadsworth, A.; Chen, H.; Thorley, K. J.; Cendra, C.; Nikolkka, M.; Bristow, H.; Moser, M.; Salleo, A.; Anthopoulos, T. D.; Sirringhaus, H.; McCulloch, I. Modification of Indacenodithiophene-Based Polymers and Its Impact on Charge Carrier Mobility in Organic Thin-Film Transistors. *J. Am. Chem. Soc.* **2020**, *142* (2), 652–664.

(57) Homyak, P.; Liu, Y.; Liu, F.; Russel, T. P.; Coughlin, E. B. Systematic Variation of Fluorinated Diketopyrrolopyrrole Low Bandgap Conjugated Polymers: Synthesis by Direct Arylation Polymerization and Characterization and Performance in Organic Photovoltaics and Organic Field-Effect Transistors. *Macromolecules* **2015**, *48* (19), 6978–6986.

(58) Ning, L.; Han, G.; Yi, Y. Conformational and Aggregation Properties of PffBT4T Polymers: Atomistic Insight into the Impact of Alkyl-Chain Branching Positions. *J. Mater. Chem. C* **2019**, *7* (45), 14198–14204.

(59) Gupta, S.; Chatterjee, S.; Zolnierzuk, P.; Nesterov, E. E.; Schneider, G. J. Impact of Local Stiffness on Entropy Driven Microscopic Dynamics of Polythiophene. *Sci. Rep.* **2020**, *10*, 9966.

(60) Liu, J.; Shao, S.; Wang, H.; Zhao, K.; Xue, L.; Gao, X.; Xie, Z.; Han, Y. The Mechanisms for Introduction of N-Dodecylthiol to Modify the P3HT/PCBM Morphology. *Org. Electron.* **2010**, *11* (5), 775–783.

(61) Wen, Y. H.; Lin, P. C.; Hua, C. C.; Chen, S. A. Dynamic Structure Factor for Large Aggregate Clusters with Internal Motions: A Self-Consistent Light-Scattering Study on Conjugated Polymer Solutions. *J. Phys. Chem. B* **2011**, *115* (49), 14369–14380.

(62) Steyrleuthner, R.; Schubert, M.; Howard, I.; Klaumünzer, B.; Schilling, K.; Chen, Z.; Saalfrank, P.; Laquai, F.; Facchetti, A.; Neher, D. Aggregation in a High-Mobility n-Type Low-Bandgap Copolymer with Implications on Semicrystalline Morphology. *J. Am. Chem. Soc.* **2012**, *134* (44), 18303–18317.

(63) Ding, L.; Wang, Z.-Y.; Yao, Z.; Liu, N.; Wang, X.-Y.; Zhou, Y.; Luo, L.; Shen, Z.; Wang, J.; Pei, J. Controllable Transformation between the Kinetically and Thermodynamically Stable Aggregates in a Solution of Conjugated Polymers. *Macromolecules* **2021**, *54* (12), 5815–5824.

(64) West, W.; Pearce, S. The Dimeric State of Cyanine Dyes. *J. Phys. Chem.* **1965**, *69* (6), 1894–1903.

(65) Yang, Y. C.; Ward, J. R.; Seiders, R. P. Dimerization of Cobalt(II) Tetrasulfonated Phthalocyanine in Water and Aqueous Alcoholic Solutions. *Inorg. Chem.* **1985**, *24* (12), 1765–1769.

(66) Würthner, F.; Yao, S. Dipolar Dye Aggregates: A Problem for Nonlinear Optics, but a Chance for Supramolecular Chemistry. *Angew. Chemie Int. Ed.* **2000**, *39* (11), 1978–1981.

(67) Bi, Z.; Naveed, H. B.; Mao, Y.; Yan, H.; Ma, W. Importance of Nucleation during Morphology Evolution of the Blade-Cast PffBT4T-2OD-Based Organic Solar Cells. *Macromolecules* **2018**, *51* (17), 6682–6691.

(68) Ponder, J. F., Jr.; Chen, H.; Luci, A. M. T.; Moro, S.; Turano, M.; Hobson, A. L.; Collier, G. S.; Perdigão, L. M. A.; Moser, M.; Zhang, W.; Costantini, G.; Reynolds, J. R.; McCulloch, I. Low-Defect, High Molecular Weight Indacenodithiophene (IDT) Polymers Via a C–H Activation: Evaluation of a Simpler and Greener Approach to Organic Electronic Materials. *ACS Mater. Lett.* **2021**, *3* (10), 1503–1512.

(69) Xiao, M.; Kang, B.; Lee, S. B.; Perdigão, L. M. A.; Luci, A.; Warr, D. A.; Senanayak, S. P.; Nikolkka, M.; Statz, M.; Wu, Y.; Sadhanala, A.; Schott, S.; Carey, R.; Wang, Q.; Lee, M.; Kim, C.; Onwubiko, A.; Jellett, C.; Liao, H.; Yue, W.; Cho, K.; Costantini, G.; McCulloch, I.; Sirringhaus, H. Anisotropy of Charge Transport in a Uniaxially Aligned Fused Electron-Deficient Polymer Processed by Solution Shear Coating. *Adv. Mater.* **2020**, *32* (23), 2000063.

□ Recommended by ACS

Dynamics of Preaggregation and Film Formation of Donor–Acceptor π -Conjugated Polymers

Yuta Yabuuchi, Masanori Ozaki, *et al.*

DECEMBER 22, 2021

ACS MATERIALS LETTERS

READ 

Understanding Solution State Conformation and Aggregate Structure of Conjugated Polymers via Small Angle X-ray Scattering

Justin J. Kwok, Ying Diao, *et al.*

MAY 19, 2022

MACROMOLECULES

READ 

Solvent Role in the Self-Assembly of Poly(3-alkylthiophene): A Harmonic Light Scattering Study

Michèle Moris, Thierry Verbiest, *et al.*

FEBRUARY 12, 2021

MACROMOLECULES

READ 

Role of Molecular Weight in Microstructural Transition and Its Correlation to the Mechanical and Electrical Properties of P(NDI2OD-T2) Thin Films

Kefeng Zhao, Yanchun Han, *et al.*

OCTOBER 29, 2021

MACROMOLECULES

READ 

Get More Suggestions >